



Contents lists available at ScienceDirect

## Combustion and Flame

journal homepage: [www.elsevier.com/locate/combustflame](http://www.elsevier.com/locate/combustflame)

# A molecular dynamics simulation investigation of fuel droplet in evolving ambient conditions



Hiromichi Yanagihara<sup>a,b</sup>, Igor Stanković<sup>a,c,\*</sup>, Fredrik Blomgren<sup>d</sup>, Arne Rosén<sup>d</sup>, Ichiro Sakata<sup>a</sup>

<sup>a</sup> Research & Development, Toyota Motor Europe NV/SA, B-1930 Zaventem, Belgium

<sup>b</sup> ODY Co. Ltd., Musashino, Tokyo, Japan

<sup>c</sup> Scientific Computing Laboratory, Institute of Physics Belgrade, University of Belgrade, 11080 Belgrade, Serbia

<sup>d</sup> Chalmers Industrial Technologies, Chalmers Science Park, SE-412 88 Göteborg, Sweden

## ARTICLE INFO

### Article history:

Received 31 January 2013

Received in revised form 22 May 2013

Accepted 5 September 2013

Available online 15 October 2013

### Keywords:

Spray

Evaporation

Combustion chemistry

Molecular dynamics

## ABSTRACT

Molecular dynamics simulations are applied to model fuel droplet surrounded by air in a spatially and temporally evolving environment. A numerical procedure is developed to include chemical reactions into molecular dynamics. The model reaction is chosen to allow investigation of the position of chemical reactions (gas phase, surface, liquid phase) and the behavior of typical products (alcohols and aldehydes). A liquid droplet at molecular scale is seen as a network of fuel molecules interacting with oxygen, nitrogen, and products of chemical fuel breakdown. A molecule is evaporating when it loosens from the network and diffuses into the air. Naturally, fuel molecules from the gas phase, oxygen and nitrogen molecules can also be adsorbed in the reverse process into the liquid phase. Thus, in the presented simulations the time and length scales of transport processes – oxygen adsorption, diffusion, and fuel evaporation are directly determined by molecular level processes and not by model constants. In addition, using *ab initio* calculations it is proven that the reaction barriers in liquid and gas phases are similar.

© 2013 The Combustion Institute. Published by Elsevier Inc. All rights reserved.

## 1. Introduction

Modeling of spray evaporation attracts much interest due to its significance for spray and combustion engineering applications. The theories of evaporation have been developed and improved over the last 100 years following the Maxwell paper [1]. Even today, the issue of primary interest in theoretical approaches is mass transfer of vapor quantized through evaporation and mass transport rates of the vapor molecules. There are two reasons for this. First, theory is relatively simple, and omits effects on the level of a single spray droplet, which are known to be important but hard to estimate. Second, experiments have mostly been restricted to observations of a spray as a whole, since it is hard to measure features important for the evaporation of a single droplet under realistic conditions. As a result, studies are usually focused on the evaluation of effects as an integral part of a wider problem of the spray dynamics [2–8]. A disadvantage of this approach is that complex interactions at the surface of an evaporating droplet that include heat transfer and chemical reactions are studied indirectly.

In contrast to the articles referenced above, evaporation was recently explored at level of a single droplet in a systematic way in

several experimental and modeling studies. Fang and Ward, achieved a breakthrough in understanding heat transfer influence, with a series of very precise measurements of temperature distribution near an evaporating surface, see Ref. [9]. In Refs. [10–13] models for droplet heating and evaporation have been developed. These models include convective and radiative heating of single droplets, and effects of the recirculation inside droplets. Another line of research is dedicated to convective burning of droplets. Raghavan et al. [14] have made experimental and numerical investigations of a droplet burning in a convective environment. Wu and Sirignano [15] have analyzed transient behavior of an isolated convecting burning droplet. They have considered effects of droplet surface regression, deceleration due to the drag of the droplet, internal circulation inside the droplet, non-uniform surface temperature, and effect of surface tension. An initial envelope flame was found to persist in time, and an initial wake flame was always transitioned into the envelope flame at a later time, with the normalized transition delay controlled by the initial Reynolds number and the initial Damköhler number [15,16]. The moment of transition is postponed further into the lifetime for smaller initial droplet radius, greater initial Reynolds number, or smaller initial Damköhler number.

Localized ignition of droplet-laden flows is important for direct-injection internal combustion engines. An example of combustion concepts currently under development is homogeneous charged

\* Corresponding author at: Scientific Computing Laboratory, Institute of Physics Belgrade, University of Belgrade, 11080 Belgrade, Serbia.

E-mail address: [igor.stankovic@ipb.ac.rs](mailto:igor.stankovic@ipb.ac.rs) (I. Stanković).

compression ignition (HCCI), expected to lead to low NO<sub>x</sub> and smoke emissions without after treatment and with increased energy efficiency [7,17]. A great concern of HCCI engine design is how to control the start of combustion, evolution, and rate, once fuel is injected into the engine cylinder. For lean mixtures, HCCI has successfully controlled this process [17], but richer operation conditions remain a challenge (still lean but close to stoichiometry). A reason for this is that degree of pre-evaporation at ignition point, the number density of droplets, their chemical composition and droplet size are important parameters. A control of ignition delay is also important for control of combustion process. It is observed that it is easier to ignite droplet-laden mixtures than lean pre-vaporized mixtures. In droplet-laden mixtures, it is easier to control locally stoichiometric ratio as the droplets evaporate and obtain time resolved heat release [6,7]. Numerical simulations show that evaporative cooling in sprays can delay ignition, and that ignition delay is extended with decreasing droplet size [18]. Also, it is reasonable to assume that oxidation reactions take place in both liquid and gas phase. Current CFD simulations of droplet auto-ignition assume that most reactions in early stages of ignition take place close to the liquid surface where concentration of fuel molecule is the highest [19]. This could be a potential tackling point for the control of combustion. The first reaction of the fuel with oxygen produces peroxy radicals, cf. Ref. [20]. With the increase of temperature without presence of additional oxygen, peroxy radical will decompose to more stable chemical species [7,20]. A distinct acceleration of ignition process is expected, according to Warnatz et al. [20], as a result of the second oxygen reaction with peroxy radical. One can imagine combustion scheme, which utilizes molecular scale processes: If the injection point is selected at sufficiently high pressure and low temperature (e.g., by intake pressure boosting), evaporation rate would be moderate and oxygen would be spread by the diffusion throughout droplet and in that way come into the contact with fuel. The result would then be a kind of stable mixture of oxygen and fuel.

Although droplet evaporation has been a research topic for several decades, studies dealing with molecular aspects of the droplet interaction with the environment are rare and mainly intended to explore evaporation of noble gases and small molecules [21,22]. The first molecular dynamics study of argon droplet vaporization under subcritical conditions was done by Long et al. [23]. It was followed by a simulation of liquid oxygen vaporizing under supercritical conditions [24] and water [25]. Consolini et al. [26] studied the evaporation of xenon droplets in a nitrogen environment under subcritical and supercritical conditions. Only recently in two separate studies, the simulations of n-heptane droplet vaporization were performed [27] and behavior of diffusion coefficient and clustering were investigated for n-alkanes in critical conditions [28].

We demonstrate in this work how molecular dynamics simulations can augment spray modeling and experiments at small length scales. Iso-octane is chosen as the liquid molecule interacting with gas (air) phase. Nevertheless processes and observed dynamical behavior should be generic to all liquid alkanes and their mixtures. We explore, if the first reaction of fuel molecules with oxygen could also take place in the liquid phase, and how the reaction products interact with the discrete molecular structure of the surface, i.e., their absorption, diffusion, and evaporation. Non-equilibrium molecular dynamics simulations use parameters obtained directly from *ab initio* considerations and do not require additional sub-models. However, a method of coarsening the scale and extracting conclusions from molecular simulation results to meso-scale or to continuum description is not obvious. At molecular level, one can observe molecules adsorbed onto the surface and fluxes of molecules penetrating from the surface into the liquid core (air molecules, surface reaction products). At scales under 0.1 μm, the fuel droplet surface is a network of fuel molecules, at-

tached by intermolecular forces to their neighbors and in contact with air. A molecule is evaporating when it loosens from the network and diffuses into the air. Naturally, fuel molecules from the gas phase, oxygen and nitrogen molecules can also absorb into the liquid phase in a reverse process. *The strategy in this paper is based on calculating molecular fluxes and relating them to macroscopically observable quantities or processes, which determine the quality of combustion.* This allows us to introduce differentiation between molecular adsorption and absorption. Molecular adsorption is seen in simulations as adhesion from a gas to a surface and absorption is following process in which a molecule fluid permeates (diffuses) into a liquid core. *Since currently no single continuum model or simulation algorithm can encompass the range of length scales between molecular and meso-scales, the goal of the present work is set to study directly at molecular scale interaction of evaporation, diffusion, as well as, liquid and gas phase chemistry.*

The paper is organized as follows. Section 2 gives an overview of molecular dynamics approach used in this work. The formulation of model reaction is presented in Section 3. The results of all the simulations are presented in Section 4, followed by conclusions in final Section 5.

## 2. Approach to molecular evaporation

Non-equilibrium molecular dynamics (NEMD) simulations were developed as routine solutions of Newton's equations and in the meantime applied to simulate the motions of atoms and molecules in both solid, liquid, and gaseous materials [29–34]. The intermolecular and intramolecular forces are parameterized by incorporating quantum effects in the parameters of the potential function [35–38]. The classical equations of motion of Newton's mechanics are integrated with the force acting on each molecule obtained from the potential energy derivative. The position, velocity, and orientation of each molecule in the system is known at each instance of time. In this way, complex molecular phenomena can be studied and at the same time computationally expensive *ab initio* quantum mechanical calculations are avoided.

The NEMD simulations are performed using molecular dynamics code MDynamix [29]. The force field used in this work is TraPPE (Transferable Parameters for Phase Equilibria) which is shown to produce accurate results for the types of molecules of interest, i.e., branched alkanes, aldehydes and alcohols [35–38]. In the TraPPE force field, CH<sub>x</sub> groups, e.g., methyl and methylene, are modeled as pseudoatoms located at the sites of the carbon atoms, whereas all other atoms (hydroxyl O and H) are introduced explicitly. The non-bonded interactions are described by pairwise-additive Lennard–Jones potential and Coulomb interactions of charges:

$$u(r_{ij}) = 4\epsilon_{ij} \left[ \left( \frac{\sigma_{ij}}{r_{ij}} \right)^{12} - \left( \frac{\sigma_{ij}}{r_{ij}} \right)^6 \right] + \left[ \frac{q_i q_j}{4\pi\epsilon_0 r_{ij}} \right] \quad (1)$$

where  $r_{ij}$  is the distance between atoms and CH<sub>x</sub> group, and  $\epsilon_{ij}$ ,  $\sigma_{ij}$ ,  $q_i$ , and  $q_j$  Lennard Jones potential well depth, size of the atom or CH<sub>x</sub> group, and partial charges, respectively, for the pair of atoms and/or pseudo atoms  $i$  and  $j$ . A harmonic potential is used to control bond angle  $\theta$  bending around equilibrium bending angle  $\theta_0$

$$u_{bend} = \frac{k_\theta}{2} (\theta - \theta_0)^2 \quad (2)$$

where  $k_\theta$  is force constant. The parameters used in this work are listed in Table 1.

Having specified the potential energy function  $V(r_N) = \sum_i u(r_{ij}) + \sum_{bonds} u_{bend}$ , the next step is to calculate the atomic forces  $F_i = -\partial V(r_N) / \partial r_i$  and use them to integrate the equation of motion. The output of such a simulation is the position and velocity of each molecule in the system. In order to reduce calculation time, we use

**Table 1**

Parameters for the TraPPE force field. Charges are different for sites adjacent to the alcohol oxygen and aldehyde carbon, and otherwise zero [35–38].

Bond length	Pseudoatom	$r_0$ (Å)		
CH <sub>x</sub> –CH <sub>y</sub>	all	1.54		
CH <sub>x</sub> –OH	alcohol	1.43		
CH=O	aldehyde	1.217		
O–H		0.945		
$u(r_{ij})$ , (Eq. 1)	Molecule	$\sigma$ (Å)	$\epsilon/k_B$ (K)	q
CH <sub>2</sub> (sp <sup>3</sup> )	Alcohol/aldehyde	3.95	46.0	+0.265/–0.043
CH (sp <sup>3</sup> )	Alcohol	4.33	10.0	+0.265/–0.043
C (sp <sup>3</sup> )	Alcohol	5.80	0.5	+0.265
CH <sub>3</sub> (sp <sup>3</sup> )	All other	3.75	98.0	0
CH <sub>2</sub> (sp <sup>3</sup> )	All other	3.95	46.0	0
CH (sp <sup>3</sup> )	All other	4.68	10.0	0
C (sp <sup>3</sup> )	All other	6.40	0.5	0
O	Alcohol	3.02	93.0	–0.700
H	Alcohol			+0.435
CH (sp <sup>2</sup> )	Aldehyde	3.52	54.0	+0.525
O (sp <sup>2</sup> )	Aldehyde	3.05	79.0	–0.482
$u_{bend}$ (Eq. 2)		$\theta_0$ (°)	$k_0/k_B$ (K)	
CH <sub>x</sub> –CH <sub>2</sub> –CH <sub>y</sub>		114	62500	
CH <sub>x</sub> –CH–CH <sub>y</sub>		112	62500	
CH <sub>x</sub> –C–CH <sub>y</sub>		109.47	62500	

cut off radius for the interactions so that atom pairs whose distances are greater than the cutoff have interaction energy zero. We use cutoff radius of 30Å which is roughly 5 $\sigma$ , cf. Table 1. The resulting energy calculation error is less than  $u/k_B = 0.5$  mK, i.e., many orders of magnitude smaller than kinetic energy of the molecule. Therefore introduction of cut-off radius should not have any significant influence on simulation results. We use the canonical NVT ensemble in our molecular dynamics simulations, in which moles (N), volume (V) and temperature (T) are conserved. In NVT ensemble, the energy of endothermic and exothermic processes are exchanged with a thermostat. The central idea of thermostat methods is to simulate in such a way that we obtain a canonical distribution by adding and removing kinetic energy from molecules in NEMD system. We have used a popular and deterministic Nosé–Hoover thermostat in this work [39,40]. From this output a number of properties and phenomena can be calculated and understood, e.g., thermodynamic properties and transport properties, etc.

We introduce a molecular level analogue to Damköhler number ( $Da$ ) used in fluid dynamics in order to study interplay between oxygen molecules adsorption and chemical reactions in the surface. A ratio of the total flux of oxygen species molecules that come into the surface  $J_{O_2,outer}$  and the reaction rate  $k$  is used:

$$Da^{MD} = \frac{k[C_8H_{18}][O_2]}{J_{O_2,outer}S}, \quad (3)$$

where  $[C_8H_{18}]$  and  $[O_2]$  are concentrations of iso-octane and oxygen, respectively and  $S$  is surface, cf. Fig. 3. The reaction  $k$  is defined by the standard Arrhenius expression, i.e.,  $k = Ae^{-E_A/k_B T}$ , where  $A$  is prefactor,  $k_B$  Boltzmann constant and  $E_A$  activation energy.

The simulation procedure to include chemical reactions is as follows: the simulations are stopped at regular intervals (every 25 ps) and the distances between all oxygen and iso-octane molecules are calculated. Depending on chosen reaction rate, a number of the closest oxygen/iso-octane molecule pairs are chosen to react and replaced by one aldehyde ( $C_4H_8O$ ) and one alcohol ( $C_4H_{10}O$ ) fragment. After reaction, the fragments should roughly occupy the same volume as the removed fuel molecule. To achieve this, fragments are placed at the position of parts of iso-octane molecule from which they originated and aligned with them, i.e., overlap of Cartesian coordinates between fragments and removed fuel molecule maximized. This is done outside molecular dynamics code

MDynamix [29] using a script, see Fig. 4. After fuel/oxygen molecules are removed and replaced with fragments, the system is equilibrated for 2 picoseconds in order to allow fragments to reach local energy minimum. Then the simulation is started again and run for a period of time (i.e., 25 ps) after which the above procedure is repeated again. We have performed NEMD computer simulations with about 6000 iso-octane ( $C_8H_{18}$ ) molecules and  $10^5$  air molecules (79% nitrogen and 21% oxygen molecules).

In order to evaluate the choice of NEMD potential parameters for iso-octane liquid densities, heat capacities, latent heats and vapor pressures are calculated at different temperatures. From Fig. 1, one can observe that experimental value of density of liquid iso-octane, cf. Ref. [41], compares well with simulation results. Since in this work we aim to explore processes at the surface of an evaporating droplet, the simulations are set up to calculate vapor pressures at different temperatures. The idea is to start with a box containing liquid–air interface. As the simulation progresses, fuel molecules will start to evaporate until stationary state is reached between evaporation of iso-octane molecules and adsorption rates to liquid phase is reached. Partial pressure of fuel molecules in vapor phase at the stationary state is equal to the vapor pressure. Results of the simulations are shown in Fig. 2. For wide range of temperatures, the present molecular dynamics simulations with TraPPE force field reproduce well vapor pressure values obtained in experiment, cf. Ref. [42]. Using simulation data obtained for internal energy  $U$  and volume  $V$  for bulk gas and liquid, at same temperature and pressures, latent heat is calculated using expression,

$$\Delta H_{vap} = (U_{liquid} - U_{gas}) + P(V_{liquid} - V_{gas}). \quad (4)$$

The experimental values of latent heat at 298 K and 372 K are 35.1 kJ/mol and 30.79 kJ/mol, respectively, cf. Ref. [44]. From our simulations we have obtained 34.81 kJ/mol at 298 K and 28.5 kJ/mol at 372 K.

Since heat capacity has two components (intermolecular and intramolecular) that are roughly equal in size, quantum

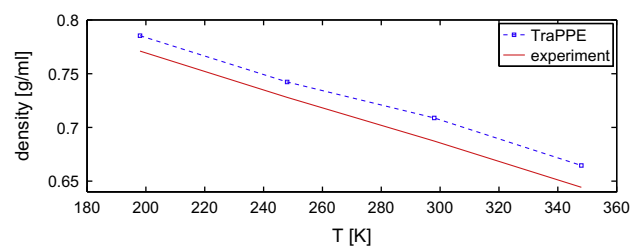


Fig. 1. Comparison of evolution of density obtained from simulation with TraPPE force field and experiment [41].

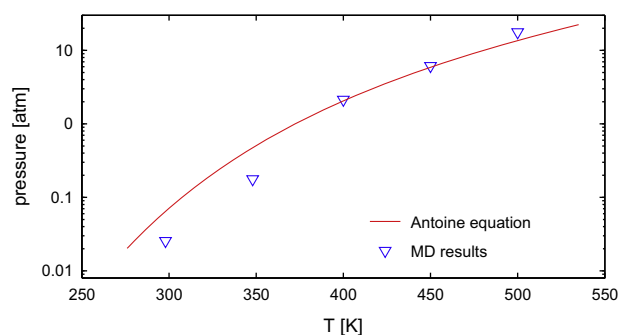
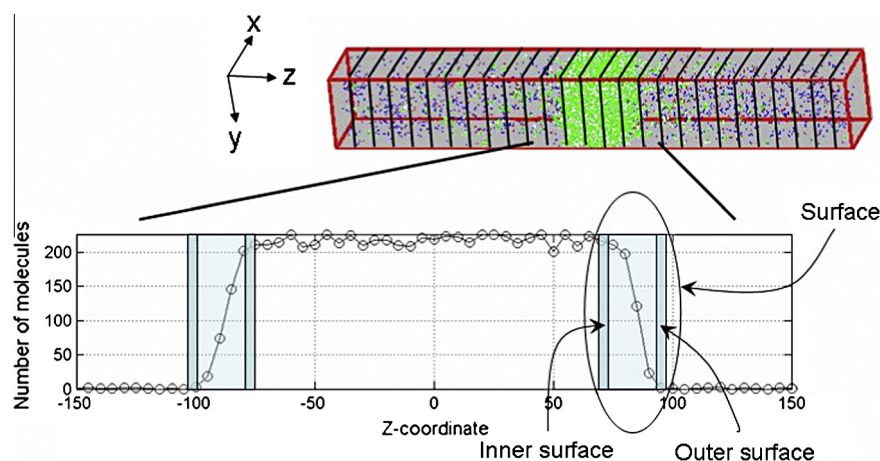


Fig. 2. Comparison of evolution of vapor pressure obtained from molecular dynamics simulations with TraPPE force field and experiment [42].



**Fig. 3.** Graphical definition of a droplet with the inner bulk liquid, surface showing an inner and outer surface slice. The whole system is surrounded by air. A surface slice is magnified to show in and outward diffusion of species.

mechanical calculations are performed in addition to the NEMD calculations. The standard way of calculating intramolecular energy is used (geometry optimization, vibrational frequency calculation followed by statistical mechanics). Quantum mechanical calculations of intramolecular energy are performed within framework of the Density Functional Theory (DFT) [43]. We use GAMESS program for electronic structure calculations with B3LYP (Becke, 3-parameter, Lee–Yang–Parr) exchange correlation functional and 6-31G\*\* basis set for molecular orbitals. The intermolecular part of the heat capacity is calculated using NEMD simulations. The heat capacity is then calculated by adding intra- and intermolecular energies and pressure volume work at a couple of temperatures, fitting the values to a function of temperature and taking the derivative with respect to temperature of that function. The experimental value for the heat capacity of isooctane at 298 K is 239.1 J/mol K [44] and the obtained simulated value (using NEMD and quantum chemistry) is 232.1 J/mol K. By comparison of heat capacity, vapor pressure, latent heat, and density calculated with TraPPE force fields and other force fields found in literature, one can conclude that obtained values reproduce experimental results with a reasonable accuracy [44,45].

A schematic of computational domain is shown in Fig. 3. The droplet is simulated in a rectangular geometry using periodic boundary conditions, where isooctane molecules are placed in the center surrounded by air (oxygen and nitrogen). The liquid phase iso-octane molecules (green<sup>1</sup>) are in the center of the simulation box. The width and height of the liquid droplet surface are 100 Å, and depth of liquid phase at on-set of simulation is 150 Å. The droplet is surrounded by air at beginning of the simulations. Later in the course of the simulation, the droplet is surrounded by mixture of air and fuel molecules as result of the evaporation. The plot in Fig. 3, shows the number of fuel molecules as a function of Z-coordinate. The interface between gas and liquid phase is not flat. The local density drops from a high value to a low value as we go from the center of the droplet outwards to the gas phase. We define two surfaces orthogonal to z-axis, inner (at 95% of liquid phase density) and outer surface (5% liquid phase density). Between inner and outer surface density is gradually changing. The region inside inner surface is called the liquid phase, the outside region is the gas phase, and narrow region between two surfaces is called surface region.

We have performed simulations with controlled overall temperature and volume. The pressure increases as result of tempera-

ture increase and decreasing volume of the gas phase. We choose to simulate the compression by raising the temperature and pressure stepwise every 250 ps of the simulation according to an adiabatic compression curve (cf. Table 2). That period of time was sufficiently long for the system to reach a stationary state and to collect enough data to calculate averages for transport coefficients. The reason is molecular frequency of collisions which is of the order of 10 ps in the gas phase at 300 K and 3 atm.

### 3. Model reaction

Due to the fact that there are no quantum chemical calculations involved in the NEMD-simulations, it is not standard to include chemical reactions. Before going into details of the model reaction used in present work, we explore if and how the factors of environment (gas, liquid) influence the chemical reactions. The chemical reaction with the concomitant breaking/formation of bonds and redistribution of electrons are quantum phenomenon by nature. We have therefore performed quantum chemical calculations of the reaction between alkane and oxygen molecule in the gas phase and in the bulk fuel region. In the fuel bulk, the solvent effects are present (interactions of both reacting molecules with other molecules in vicinity). The GAMESS code for density functional theory (DFT) calculations with B3LYP/6-31G\*\* level of theory is used. The DFT and more especially B3LYP functional has been recognized as a good method for modeling of the reactions in which whatever abstracting radical (oxygen, oxyl or alkyl) interacts with either alkane, amine, or alcohol, cf. Ref. [46–49]. In order to reduce calculation effort, we used ethane (C<sub>2</sub>H<sub>6</sub>) molecule instead of iso-octane for the following two reasons: the quantum interaction length is comparable to the chemical bond length size and oxygen interacts only with CH<sub>x</sub> groups in its vicinity. Also values of the hydrogen abstraction activation energies for different alkanes found in literature [50–57] are similar and in the range 190–230 kJ/mol. Full reaction path calculations, from reactants through transition state finally to products, are performed for a hydrogen abstraction reaction between oxygen (O<sub>2</sub>) and ethane, which we take as a model reaction. The result is shown in Fig. 5. The molecular and atomic arrangement is shown at various points on the potential energy surface starting from the left with reactants and ending to the right with products. The reaction index, used as abscissa in Fig. 5, has no real physical meaning other than the fact that different reaction indices represent different molecular and atomic arrangements, and only size of the reaction barrier in two cases is important for analysis. It can be seen that the reaction barrier, i.e., activation

<sup>1</sup> For interpretation of color in Fig. 3, the reader is referred to the web version of this article.

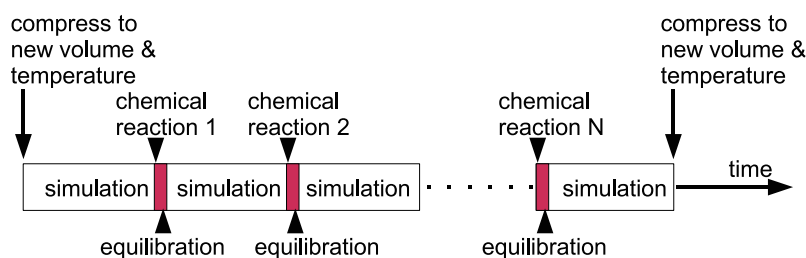


Fig. 4. Graphical representation of the procedure for performing simulations including chemical reactions.

Table 2

Temperature and pressure stepwise every 250 ps of the simulation according to adiabatic compression curve. Evaporation rates are calculated from data in Fig. 7d.

T [K] (P [atm])	Averaging time period	$r_{\text{vap}}$ [molecules/(nm <sup>2</sup> ns)]	mol/(m <sup>2</sup> s)
298 (1)	0–250 ps	5.8	96
326 (1.4)	250–500 ps	102	170
356 (1.9)	500–750 ps	218	360
389 (2.6)	750–1000 ps	726	1210
426 (3.5)	1000–1250 ps	1434	2380
465 (4.8)	1250–1500 ps	2468	4100

energy, is  $E_A = 197$  kJ/mol in the gas phase. The calculated activation energy is in agreement with the value found in literature, cf. Ref. [57]. In the liquid phase activation energy is  $E_A = 190$  kJ/mol and essentially the same as activation energy in the gas phase. Since almost all other reactions (i.e., forming several peroxy radicals  $\text{C}_2\text{H}_5\text{OO}^*$  and eventually hydroxyl radical) have lower reaction barriers than hydrogen abstraction, it is reasonable to expect that they will be even less sensitive to the surfactant effect. Therefore, we assume that any difference in reaction probability between the liquid and gas phases is governed by collision frequency.

In this work, a model reaction is introduced into NEMD simulations to study the spatial distribution of chemical reactions in the liquid phase, transport of products and reactants in the system as whole, and how chemical reactions affect the structure of the droplet. Though hydrogen abstraction is the first reaction in the reaction chain, the hydrogen abstraction is not the primary route for formation of the radical ( $\text{C}_2\text{H}_5^*$ ) due to its high endothermicity. Once the reactions have sufficiently progressed and the system

has accumulated enough radicals, such as OH, O, and H, and hydrogen abstraction by these radical is favored over the abstraction by molecular oxygen [57–59]. After H-abstraction step and below 1000 K, iso-octyl radical reacts further along sequence of reactions to create aldehydes, ketohydroperoxyde, and ethers [59–63]. Some of these reactions involve additional oxygen molecules and almost all have lower energy barriers than the hydrogen abstraction. In the molecular dynamics simulations, we could not systematically study influence of the whole reaction chain on the molecular structure of the droplet due to the large number of reactions. Instead, we defined a model chemical reaction as  $\text{C}_8\text{H}_{18} + \text{O}_2 \rightarrow \text{C}_4\text{H}_8\text{O} + \text{C}_4\text{H}_{10}\text{O}$  which should include features of low- and medium-temperature ( $T < 1000$  K) reactions from the reaction chain:

1. It involves fuel and oxygen molecules like reaction  $\text{C}_8\text{H}_{18} + \text{O}_2 \rightarrow \text{C}_8\text{H}_{17} + \text{OOH}$  from standard chemistry mechanisms in which the product of hydrogen abstraction from  $\text{C}_8\text{H}_{18}$  is split in two smaller stable molecules.
2. We chose a reaction rate that gives a ratio of reaction rate and oxygen flux in liquid phase (Damköhler number)  $1 < Da^{\text{MD}} < 10$ , with activation energy  $E_A = 10$  kJ/mol and Arrhenius equation prefactor  $A = 2.5 \times 10^{12}$  m<sup>3</sup>/mol,
3. Its products are an aldehyde ( $\text{C}_4\text{H}_8\text{O}$ ) and alcohol ( $\text{C}_4\text{H}_{10}\text{O}$ ) so we could study how different products of branching diffuse inside the droplet.

The activation energy is chosen sufficiently low to have dependence on temperature, and close to abstraction of hydrogen by hydroxyl radical, cf., Ref. [57,50]. Since  $Da^{\text{MD}} > 1$ , even with our choice of a very small Arrhenius prefactor oxygen molecules are going to

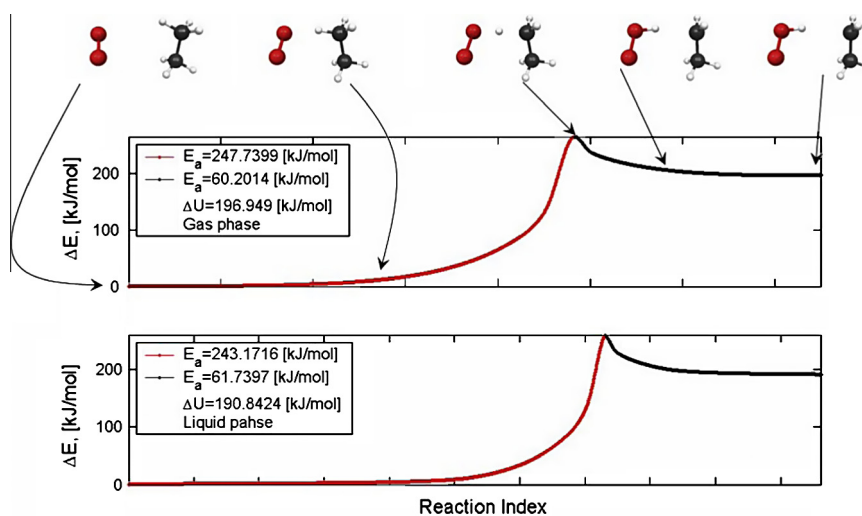


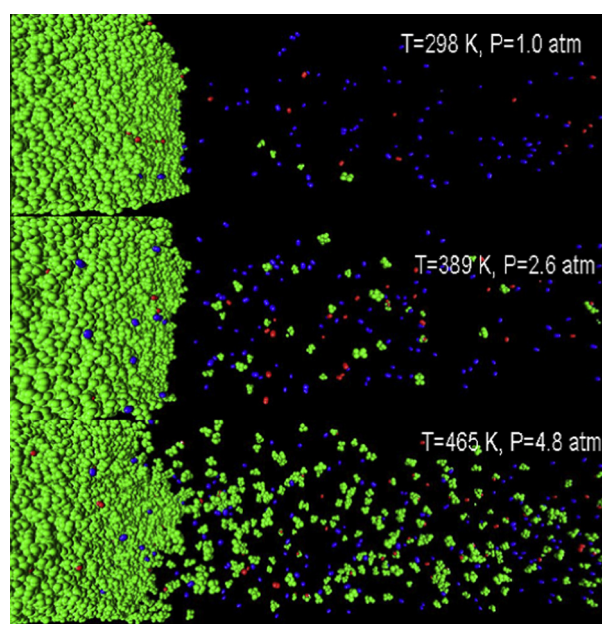
Fig. 5. Reaction path calculations for gas phase (top) and liquid phase (bottom). The reaction index used as abscissa has no real physical meaning other than the fact that different reaction indices represent different molecular and atomic arrangements.

react very fast with fuel in the surface. According to our methodology, chemical reactions take place dominantly in the surface region. This fact is not surprising considering that the collision frequency between oxygen and isooctane is higher in the surface region than in the gas phase and chosen model reaction proceeds very fast. On the other hand such choice should not be far from reality, since numerical simulations of auto-ignition of fuel droplets in air show that most pre-ignition chemical reactions take place in air close to the fuel droplet surface, see Ref. [19].

#### 4. Results

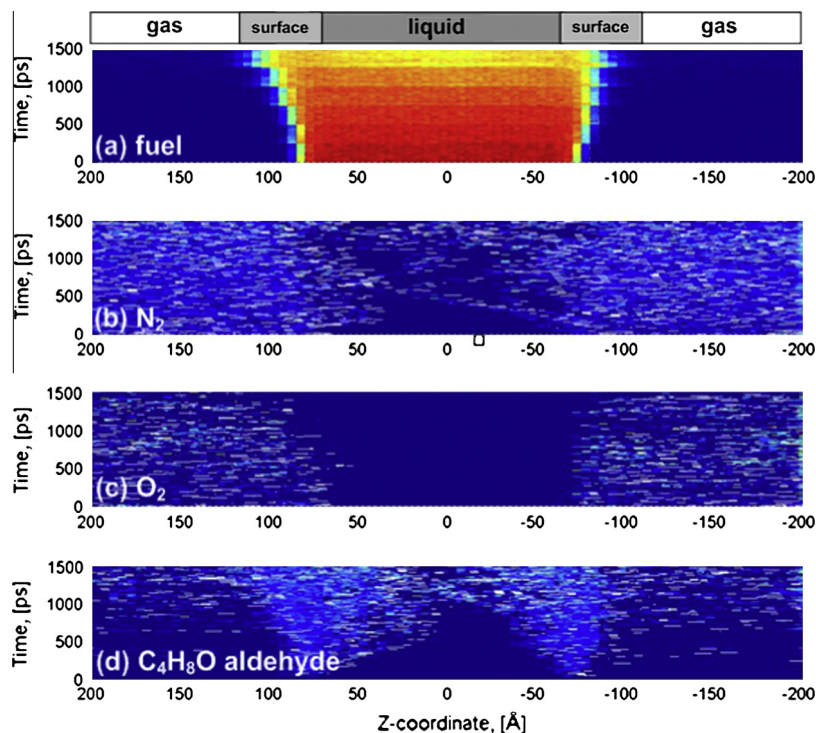
In this section we analyze NEMD simulation results of simultaneous evaporation, and adsorption and diffusion of oxygen and reaction products into liquid fuel droplet in evolving ambient conditions. Fig. 6 gives snap-shots of the simulations performed. Isooctane molecules are green, oxygen and nitrogen molecules are red and blue, respectively. To the left in Fig. 6 is the surface region. Going from the top picture to bottom, temperature and pressure are increased according to an adiabatic compression curve. As seen in the figure, molecules detach from the surface and evaporate into air. In the same Fig. 6 one can also observe oxygen (red dots) and nitrogen (blue) being adsorbed into the droplets surface and then diffusing into the bulk of the liquid fuel. The surface of the droplet does not represent a barrier for penetration of oxygen molecules into the liquid fuel bulk. This is due to the fact that the simulated intermolecular binding energy of both oxygen and nitrogen in liquid fuel is about 8 kJ/mol and therefore two times higher than its kinetic energy value at 500 K. One could expect that the fuel droplet is going to adsorb a part of the gaseous oxygen and trap it in the liquid fuel, since O<sub>2</sub> molecules will not have enough kinetic energy to leave the droplet.

Fig. 7 gives more insight into the transport processes in the surface, liquid, and gas phase. The figure shows the distribution of different species as a function of Z-coordinate (abscissa) and



**Fig. 6.** Evolution of the molecular structure at the surface of an iso-octane (green molecules) droplet during adiabatic compression. The oxygen (red) and nitrogen (blue) molecules can also be seen on the picture. The evaporation increases rapidly as the temperature approaches boiling point (at roughly  $T = 450$  K). Cross-section is 100 Å wide, snapshots for temperatures  $T = 298$  K, 389 K, and 465 K and pressures according to adiabatic curve are shown. (For interpretation of the references to color in this figure legend, the reader is referred to the web version of this article.)

time (ordinate). In Fig. 7a, the distribution of isooctane molecules is described. As temperature and pressure are increased (i.e. along the ordinate axis), the droplet expands and the fuel density decreases. Although it is not quite evident in Fig. 7, the surface region also expands. Fig. 7b and c shows the distribution of nitrogen and



**Fig. 7.** Distribution of different species (fuel, N<sub>2</sub>, O<sub>2</sub>, C<sub>4</sub>H<sub>10</sub>O) as a function of Z-coordinate and time. Temperature and pressure are increased every 250 ps stepwise in the range 298–465 K according to Table 2. The distribution of different species is represented in space Z-coordinate (abscissa) and time (ordinate). Z-coordinate is the direction going from the droplet center to the gas phase and is measured in Ångström, Z-coordinate equal to 0 corresponds to the liquid center.

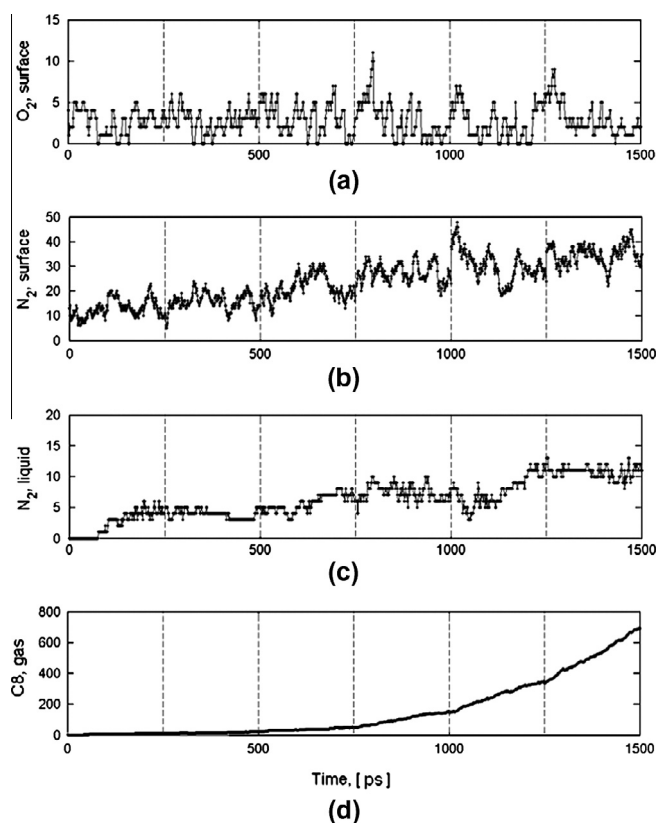


**Fig. 8.** Results of NEMD simulations with chemical reactions are shown. Number of molecules a function of time (abscissa) for (a) oxygen in droplet surface, nitrogen both in (b) liquid surface and (c) bulk, and (d) number of evaporated fuel molecules. Temperature and pressure change every 250 ps according to Table 2 (vertical lines).

oxygen respectively. Since we have chosen a high reaction rate, from Fig. 8c and d, one can see that in the surface region oxygen reacts with isoctane to create aldehyde and alcohol (products of the model chemical reaction). Nitrogen, however, does not react with isoctane and can diffuse inside the droplet, cf. Fig. 8b and c. The binding energy of  $O_2$  molecules is higher than its kinetic energy and the probability of an oxygen molecule leaving the surface falls exponentially with the ratio of the two values. Therefore, it is

expected that concentrations of oxygen molecules at liquid surface would be equal or even higher than in gas phase. From the surface, oxygen will gradually diffuse deeper into the droplet bulk. The observed adsorption rate of oxygen and nitrogen from Fig. 8 are  $100 \pm 25 \text{ mol/m}^2 \text{ s}$  and thus comparable or even higher than evaporation rate of fuel molecules at moderate pressures and high temperatures, cf. Table 2. One can expect, that the adsorption rate would scale linearly with increase of ambient pressure while the temperature is kept constant.

In Fig. 7d, the distribution of the aldehyde, one of the simulated reaction products, is shown. The distributions of aldehyde and alcohol (the other reaction product) molecules are essentially the same, which is why the latter was left out for reasons of space and clarity. Fig. 7c shows that oxygen is consumed in the surface region and, naturally, Fig. 7d therefore shows that aldehyde molecules are created in the same region. One interesting feature seen in Fig. 7d is that aldehyde molecules diffuse into the liquid phase. In addition, from Fig. 9 it can be seen that for all reactions taking place in the surface region, about 25% of the reaction products evaporate, whereas the remaining 75% remain adsorbed at the surface or diffuse into the liquid. This is more pronounced at lower temperatures. From Fig. 9, it can be also observed that aldehyde molecules are more prone to stay absorbed into the liquid phase than alcohol molecules. On the other hand, alcohol evaporates easier. The reason is the binding energies of the molecules. The molecular dynamics calculations show that alcohol-fuel binding energy is around 2.5 kJ/mol higher (considering that binding energy is negative), than the binding energy of aldehyde-fuel. At the same time kinetic energy of the aldehyde and alcohol at 450 K is roughly 3.8 kJ/mol. Therefore the evaporation rate of alcohol is higher compared to aldehyde by a factor of 2.5–1.5 depending on temperature. This is an interesting finding, since aldehydes usually have lower boiling point than corresponding alcohols, and one could expect that aldehyde molecules would evaporate faster – in this work we observe the opposite.

Diffusion rate of molecular oxygen is found to increase with temperature from  $12 \cdot 10^{-9} \text{ m}^2/\text{s}$  (298 K) to  $24 \cdot 10^{-9} \text{ m}^2/\text{s}$  (389 K), cf. Fig. 10a. The reasons for this are both increasing kinetic energy of adsorbed molecules and decreasing density of adsorbent. Calculated diffusion rate value is about one order of magnitude higher than oxygen molecule diffusion rate in water. Also from Fig. 10, we can see that diffusion rates of nitrogen, aldehyde, and

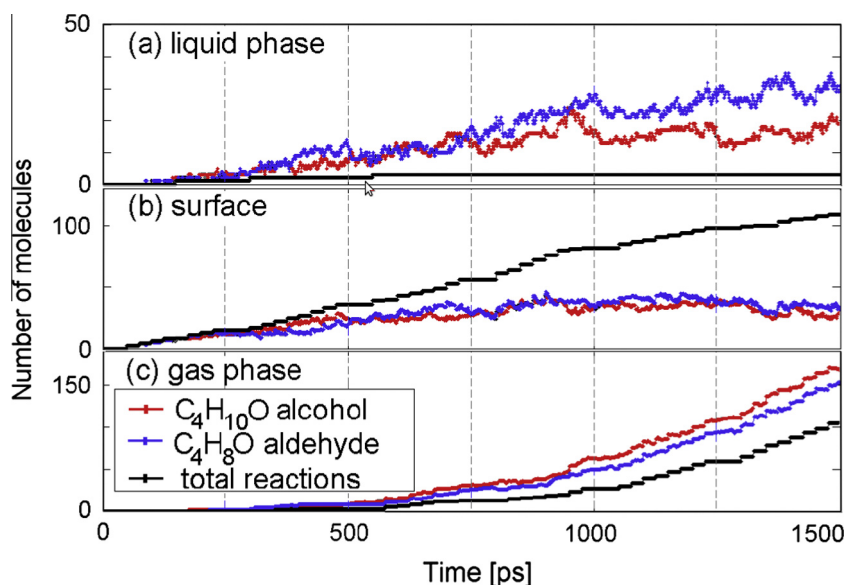


**Fig. 9.** Number of products of chemical reaction  $C_4H_{10}O/C_4H_8O$  as functions of time. Temperature and pressure are increased every 250 ps stepwise in range 298–465 K according to Table 2 (vertical lines).

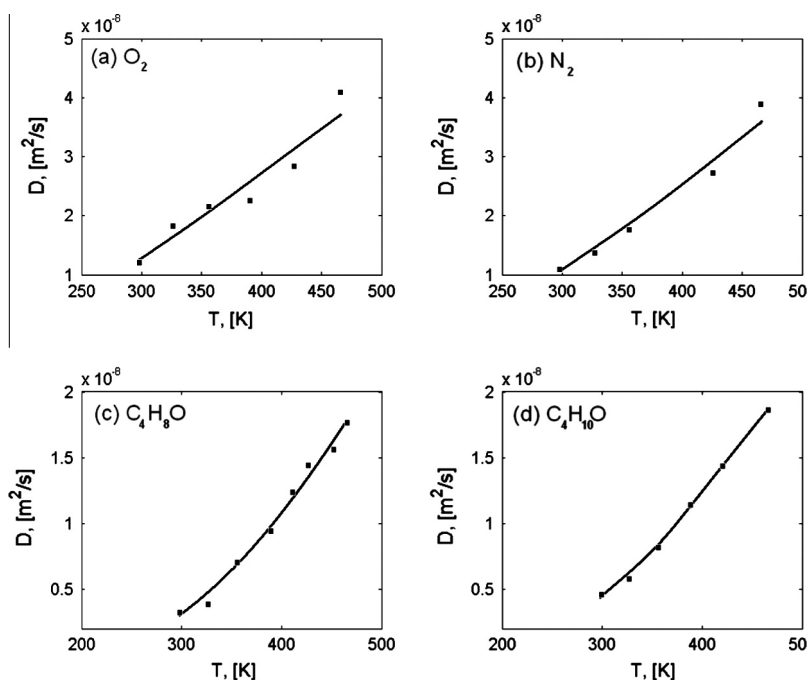


Fig. 10. Diffusion coefficients obtained from molecular dynamics simulations without chemical reactions involved in bulk liquid fuel. The evolution of diffusion coefficient with temperature is shown for (a) O<sub>2</sub>, (b) N<sub>2</sub>, (c) alcohol C<sub>4</sub>H<sub>10</sub>O, and (d) aldehyde C<sub>4</sub>H<sub>8</sub>O.

alcohol are similar to that of oxygen and scale roughly with molecular mass. This can be explained by almost one order of magnitude higher molar volume of isooctane. Compared to air, diffusion rate of molecules absorbed in liquid fuel is about two orders of magnitude smaller. From the Einstein relation for diffusion mean square displacement, we can estimate that oxygen molecules will diffuse into the center of a 10 μm (diameter) droplet, 1 ms after fuel injection and therefore at the timescale comparable with the timescale of the piston motion. Oxygen molecules diffusing into the droplet could form relatively stable reaction products containing oxygen, and stay stored in the liquid phase (and fuel rich region after the evaporation). This could be an alternative way to introduce oxygen inside the fuel, cf. Ref. [7]. In our simulations, at lower temperatures most reactions occur in the surface region. At higher temperatures, however, more isooctane molecules evaporate, resulting in an increased number of reactions taking place in the gas phase.

As the compression advances, the increase of temperature results in an exponential rise of vapor pressure close to boiling point, cf. Fig. 2. Once values of vapor and gas phase pressure become comparable pockets of fuel in gas phase are created within the droplet. Below boiling temperature, the majority of fuel molecules do not have enough energy to leave the liquid. When molecules collide, they transfer energy to each other in varying degrees, based on how they collide. Through collisions molecules can move to reduce their bonding and accumulate kinetic energy from several collisions to escape from the liquid. Due to the fact that positions and orientations of all molecules are known, it is possible to calculate evaporation rates at different simulated temperatures and pressures by simply counting the number of isooctane molecules in the gas phase. The results are shown in Fig. 8d and Table 2. The derivative of the number of molecules in the gas phase in Fig. 8d is the evaporation rate. If we calculate evaporation time of a 10 μm diameter droplet, from the Table 2, we obtain 0.1 ms at 400 K. The reason is that in the initial configuration of the present NEMD simulations there are no fuel molecules in the gas phase, resulting in two orders of magnitude higher concentration gradient than in experiment or continuum simulation, cf. Ref. [3,13,15,16,19]. Therefore, the partial pressure of fuel molecules

in gas phase was much lower than vapor pressure and evaporation advanced quicker. Considering correct prediction of latent heat and vapor pressure by TraPPE potential, different choice of initial configuration would lead to correct evaporation time. On the other hand rates of the all observed processes, would be comparably slower and thus inaccessible for NEMD study.

In order to understand effect of the pressure NEMD simulations are performed at  $P = 2.6$  and 10 atm and temperature  $T = 389$  K. The higher pressure results in higher adsorption of O<sub>2</sub> and N<sub>2</sub> molecules, see Fig. 11. The number of oxygen molecules adsorbed in

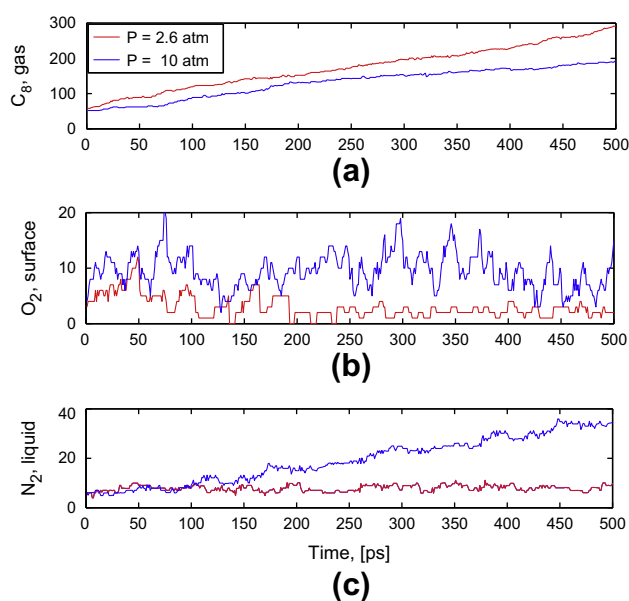
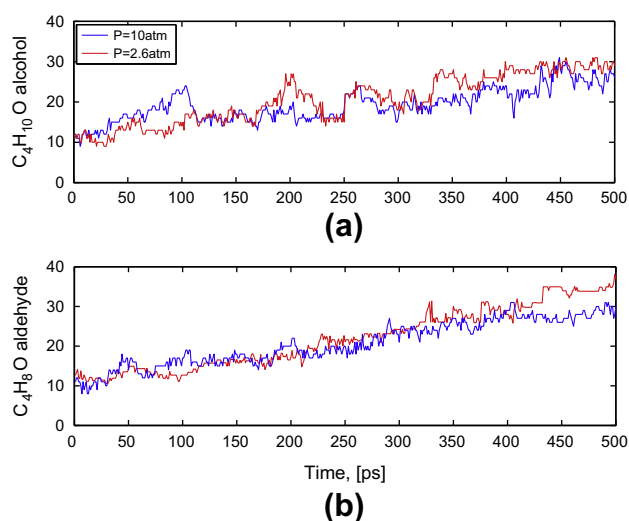


Fig. 11. Results of NEMD simulations with chemical reactions are shown at temperature  $T = 389$  K and pressures  $P = 2.6$  atm and 10 atm. Number of molecules as function of time (abscissa) for (a) fuel in gas phase, (b) oxygen in surface and (c) nitrogen in liquid phase is shown.



**Fig. 12.** Results of NEMD simulations with chemical reactions are shown at temperature  $T = 389$  K and pressures  $P = 2.6$  atm and 10 atm. Number of molecules as function of time (abscissa) for (a) alcohol  $C_4H_{10}O$  and (b) aldehyde  $C_4H_8O$  in liquid phase is shown.

droplet surface is roughly four times higher at  $P = 10$  atm than at  $P = 2.6$  atm. This is result of higher density of the  $O_2$  molecules close the droplet surface. Evaporation rate is at the same time smaller at higher pressure. One can observe steady increase in the number of  $N_2$  in liquid phase at high pressure, since reduced evaporation rate of the surface layer enables these molecules to diffuse deeper into the droplet. Since liquid phase is incompressible, there is no pressure influence on diffusion coefficients. Consequently there is no difference in diffusion of the reaction products into the liquid phase at two pressures, cf. Fig. 12.

## 5. Conclusion

We have observed at molecular scale that a liquid fuel droplet is a network of molecules, with the oxygen and products of chemical breakdown, absorbed inside. The penetration of oxygen into the surface and inside of the liquid fuel and the adsorption of reaction products is novel knowledge which reveals that the initial reactions of the pre-ignition process could also take place at the surface and inside of the liquid fuel. Quantum chemical calculations showed that there is no significant difference in hydrogen abstraction activation energy between the liquid and gas phases, which is by its own an interesting result. Even in the liquid phase, the reaction occurs in the same way as in the gas phase. The observations about evolution of molecular structure at the surface of the fuel droplet during the compression provide insight about the location and relative time scales of the processes (e.g., adsorption and diffusion of oxygen into the fuel) relevant for the molecular transport and chemistry interaction.

In summary, the current report discusses the application of molecular dynamics simulations in order to examine the initial phases of fuel/air mixing prior to the complete evaporation of droplets. The most important results are:

1. Non-equilibrium molecular dynamics calculations can be coupled with reduced chemistry. The simulations widened views on the interaction of chemistry and transport with respect to the non-equilibrium phenomena of oxygen adsorption, chemical reactions, and fuel evaporation.
2. Evaporation in this work is seen at the molecular level as a process in which fuel, air and reaction product molecules are leaving, returning and diffusing from the droplet surface. At the

surface of the fuel droplet, low temperature chemical reactions occur and reaction products containing oxygen are stored there at lower temperatures.

The molecular dynamics method showed a good potential for exploring new scientific aspects by bridging chemistry and physics with technology. The dynamical localization of different species (fuel, nitrogen, oxygen, reaction products) constitutes a novel application of NEMD to combustion problems. There is no doubt that future of internal combustion engine is related to better control of chemical energy into mechanical work. A chance to get maximal control at engineering side is offered by current developments of injector, engine boosting, and fuel sensor technology. Nevertheless, it is impossible in practice to create novel combustion design using molecular simulations as a stand alone tool due to the fact that time and length scales of combustion are out of reach for NEMD simulations. Using CFD simulations, however, these length and time scales can be simulated in the relevant way for combustion designs. Therefore, the present methodology should provide valuable inputs for novel sub-models for advanced CFD approaches. These results, together with work done by others, indicate that further investigations are appropriate [3,7,9,21,64]. Still, our ability to fully utilize its potential will depend on creation of multi-scale approaches to integrate NEMD results into CFD simulations.

## Acknowledgment

F.B. and A.R. especially thank to Jan Westergren for support and advice.

## References

- [1] J.C. Maxwell, *Philos. Trans. R. Soc. London* 170 (1879) 231.
- [2] E. Delacourt, B. Desmet, B. Besson, *Fuel* 84 (2005) 859.
- [3] J. Reveillon, F.X. Demoulin, *Proc. Combust. Inst.* 31 (2007) 2319.
- [4] A.P. Wandel, N. Chakraborty, E. Mastorakos, *Proc. Combust. Inst.* 32 (2009) 2283.
- [5] Y. Ra, R.D. Reitz, *Trans. ASME* 126 (2004) 422.
- [6] S.K. Aggarwal, *Prog. Energy. Combust. Sci.* 24 (1998) 565.
- [7] H. Yanagihara, in: P. Duret (Ed.), *New Generation of Engine Combustion*, Editions Technip, Paris, 2002, pp. 35–42.
- [8] Y. Ra, R.D. Reitz, *Int. J. Multiphase Flow* 35 (2009) 101.
- [9] G. Fang, C.A. Ward, *Phys. Rev. E* 59 (1999) 417.
- [10] B. Abramzon, W.A. Sirignano, *Int. J. Heat Mass Transfer* 32 (1989) 1605.
- [11] L.A. Dombrovsky, S.S. Sazhin, *Int. Commun. Heat Mass Transfer* 30 (2003) 787.
- [12] A.P. Kryukov, V. Yu. Levashov, S.S. Sazhin, *Int. J. Heat Mass Transfer* 47 (2004) 2541.
- [13] S.S. Sazhin, P.A. Krutitskii, W.A. Abdelghaffar, S.V. Mikhalyovsky, S.T. Meikle, M.R. Heikal, *Int. J. Heat Mass. Transfer* 47 (2004) 3327.
- [14] V. Raghavan, V. Babu, T. Sundararajan, R. Natarajan, *Int. J. Heat Mass Transfer* 48 (2005) 5354.
- [15] G. Wu, W.A. Sirignano, *Combust. Flame* 157 (2010) 970.
- [16] G. Wu, W.A. Sirignano, *Combust. Flame* 158 (2011) 2395.
- [17] R. Hasegawa, H. Yanagihara, *SAE Trans.* 112 (2003) 1070.
- [18] Y. Wang, C.J. Rutland, *Combust. Flame* 149 (2007) 353.
- [19] R. Stauch, S. Lipp, U. Maas, *Combust. Flame* 145 (2006) 533.
- [20] J. Warnatz, U. Maas, R.W. Dibble, *Combustion, fourth ed.*, Springer, Berlin, Heidelberg, DE, 2006.
- [21] R. Holyist, M. Litniewski, *Phys. Rev. Lett.* 100 (2008) 0557011.
- [22] L.G. MacDowell, P. Virnau, M. Muller, K. Binder, *J. Chem. Phys.* 120 (2004) 5293.
- [23] L.N. Long, M.M. Micci, B.C. Wong, *Comput. Phys. Commun.* 96 (1996) 167.
- [24] T.L. Kaltz, L.N. Long, M.M. Micci, J.K. Little, *Combust. Sci. Technol.* 136 (1998) 279.
- [25] M.S. Korlie, *Comput. Math. App.* 39 (2000) 43.
- [26] L. Consolini, S.K. Aggarwal, S. Murad, *Int. J. Heat Mass Trans.* 46 (2003) 3179.
- [27] A. Petrilla, M.F. Trujillo, M.M. Micci, *Atom. Sprays* 20 (2010) 581.
- [28] J.W. Mutoru, W. Smith, C.S. O'Hern, A. Firoozabadi, *J. Chem. Phys.* 138 (2013) 024317.
- [29] A.P. Lyubartsev, A. Laaksonen, *Comput. Phys. Commun.* 128 (2000) 565.
- [30] M.P. Allen, D.J. Tildesley, *Computer Simulation of Liquids*, Clarendon, Oxford, UK, 1987.
- [31] D.C. Rapaport, *The Art of Molecular Dynamics Simulations*, second ed., Cambridge University Press, Cambridge, UK, 2004.
- [32] M. Dente, S. Pierucci, E. Ranzi, G. Busani, *Chem. Eng. Sci.* 47 (1992) 2629.

- [33] M. Kroger, I. Stankovic, S. Hess, *Multiscale Model. Simul.* 1 (2003) 25.
- [34] I. Stankovic, S. Hess, M. Kroger, *Phys. Rev. E* 70 (2004) 066139.
- [35] M.G. Martin, J.I. Siepmann, *J. Phys. Chem. B* 102 (1998) 2569.
- [36] M.G. Martin, J.I. Siepmann, *J. Phys. Chem. B* 103 (1999) 4508.
- [37] B. Chen, J.J. Potoff, J.I. Siepmann, *J. Phys. Chem. B* 105 (2001) 309.
- [38] J.M. Stubbs, J.J. Potoff, J.I. Siepmann, *J. Phys. Chem. B* 108 (2004) 17596.
- [39] S. Nose, *J. Chem. Phys.* 81 (1984) 511.
- [40] W.G. Hoover, *Phys. Rev. A* 31 (1985) 1695.
- [41] A.A.H. Padua, J.M.N.A. Fareleira, J.C.G. Calado, W.A.J. Wakeham, *Chem. Eng. Data* 41 (1996) 1488.
- [42] B.E. Poling, J.M. Prausnitz, J.P. O'Connell, *The Properties of Gases and Liquids*, fifth ed., McGraw-Hill, New York, USA, 2001.
- [43] M.W. Schmidt et al., *J. Comput. Chem.* 14 (1993) 1347.
- [44] *Handbook of Chemistry and Physics*, 87th ed., Taylor & Francis, 2006.
- [45] C. Coleman, P.J. van Maaren, M. Hong, J.S. Hub, L.T. Costa, D. van der Spoel, *J. Chem. Theory Comput.* 8 (2012) 61.
- [46] D. Bertin, S. Grimaldi, M. Leblanc, S.R.A. Marque, D. Siri, P. Tordo, *J. Mol. Struct. (Theochem)* 811 (2007) 255.
- [47] H. Basch, S. Hoz, *J. Phys. Chem. A* 101 (1997) 4416.
- [48] F. Bernardi, A. Bottoni, *J. Phys. Chem. A* 101 (1997) 912.
- [49] B.S. Jursic, *Int. J. Quantum Chem.* 65 (1997) 75.
- [50] M.V. Petrova, F.A. Williams, *Combust. Flame* 144 (2006) 526.
- [51] S.C. Li, F.A. Williams, *J. Eng. Gas Turb. Power Trans. ASME* 124 (2002) 471.
- [52] S. Davis, C.K. Law, H. Wang, *Combust. Flame* 119 (1999) 375.
- [53] R.P. Lindstedt, G. Skevis, *Combust. Sci. Technol.* 125 (1997) 73.
- [54] A. Laskin, H. Wang, *Chem. Phys. Lett.* 303 (1999) 43.
- [55] B. Varatharajan, F.A. Williams, *Combust. Flame* 121 (2000) 551.
- [56] W. Tsang, *J. Phys. Chem. Ref. Data* 17 (1998) 887.
- [57] H. Machrafi, K. Lombaert, S. Cavadias, P. Guibert, J. Amouroux, *Fuel* 84 (2005) 2330.
- [58] I. Glasman, *Combustion*, third ed., Academic Press, San Diego, California, USA, 1996.
- [59] R. Ogink, *Computer Modeling of HCCI Combustion*, Ph.D. Thesis, School of Mechanical Engineering, Chalmers University of Technology, Gothenburg, Sweden, 2004.
- [60] P. Amneus, *Homogeneous Ignition – Chemical Kinetic Studies for IC-Engine Applications*, Ph.D. Thesis, Division of Combustion Physics, Lund Institute of Technology, Lund, Sweden, 2002.
- [61] H.J. Curran, P. Gaffuri, W.J. Pitz, C.K. Westbrook, *Combust. Flame* 129 (2002) 253.
- [62] E. Ranzi, P. Gaffuri, T. Faravelli, P. Dagaut, *Combust. Flame* 103 (1995) 91.
- [63] T. Faravelli, P. Gaffuri, E. Ranzi, J.F. Griffiths, *Fuel* (1998) 147.
- [64] J.B. Greenberg, *Combust. Flame* 148 (2007) 187.